Side-Supported Radial-Mode Thin-Film Piezoelectric-on-Silicon Disk Resonators

Sarah Shahraini, *Graduate Student Member, IEEE*, Mohsen Shahmohammadi, Hedy Fatemi, and Reza Abdolvand, *Senior Member, IEEE*

Abstract— **In this paper, anisotropy of single-crystalline silicon (SCS) is exploited to enable side-supported radial-mode thin-film piezoelectric-on-substrate (TPoS) disk resonators. In contrast to the case for isotropic material, it is demonstrated that the displacement of the disk periphery is not uniform for the radial-mode resonance in SCS disks. Specifically, for high-order harmonics, nodal points are formed on the edges, creating an opportunity for placing suspension tethers and enabling side-supported silicon disk resonators at the very high-frequency band with negligible anchor loss. In order to thoroughly study the effect of material properties and the tether location, anchor loss is simulated using a 3-D perfectly matched layer in COMSOL. Through modeling, it is shown that eighth-harmonic side-supported SCS disk resonators could potentially have orders of magnitude lower anchor loss in comparison to their nanocrystalline diamond (NCD) disk resonator counterparts given the tethers are aligned to the [100] crystalline plane of silicon. It is then experimentally demonstrated that in TPoS disk, resonators fabricated on an 8-μm silicon-on-insulator (SOI) wafer, unloaded quality factor improves from ~450 for the second-harmonic mode at 43 MHz to ~11 500 for the eighth-harmonic mode at 196 MHz if tethers are aligned to [100] plane. The same trend is not observed for NCD disk resonators and SCS disk resonators with tethers aligned to [110] plane. Finally, the temperature coefficient of frequency is simulated and measured for the radial-mode disk resonators fabricated on the 8-μm-thick degenerately n-type doped SCS, and the TFC data are utilized to guarantee proper identification of the harmonic radial-mode resonance peaks among others.**

Index Terms— **Anchor loss, perfectly matched layer, quality factor, radial mode, silicon disk resonator.**

I. Introduction

MICROMACHINED silicon resonators are now a growing sector of the MEMS market with applications in oscillators and sensors [1]–[3]. Regardless of the specific application, the resonator quality factor (Q) directly impacts the system performance as it basically determines the noise floor [1]. However, the optimization of quality factor is a complicated process as the physics of loss is not fully understood and hard to control in most cases. The quality factor is a measure of energy loss in a resonance system. Energy loss in resonators could be categorized into two general groups of intrinsic and extrinsic losses [4]. Intrinsic losses are principally linked to the material properties whereas extrinsic losses strongly depend on the design and implementation of the resonators. Dielectric loss ($1/Q_{\text{die}}$), phonon–phonon interaction loss ($1/Q_{p-p}$), which includes Akheiser loss [5], and thermoelastic dissipation [6] are the examples of intrinsic loss in resonators. On the other hand, anchor loss ($1/Q_{\text{anc}}$), air/fluid damping loss ($1/Q_{\text{air}}$), ohmic loss ($1/Q_{\text{ohm}}$), and interface losses ($1/Q_{\text{interface}}$) are the examples of extrinsic loss in resonators and these losses could be reduced by proper design and operation in a controlled environment (e.g., operation in partial vacuum). The overall Q of the resonator could be written as a function of these different loss components

$$\frac{1}{Q_{\text{tot}}} = \frac{1}{Q_{\text{die}}} + \frac{1}{Q_{p-p}} + \frac{1}{Q_{\text{anc}}} + \frac{1}{Q_{\text{air}}} + \frac{1}{Q_{\text{ohm}}} + \frac{1}{Q_{\text{interface}}} + \frac{1}{Q_{\text{other}}}. \quad (1)$$

From this equation, it is clear that if the quality factor associated with any of the individual sources of loss is small relative to others, then Q_{tot} would be dominated by that mechanism (i.e., the largest energy loss). At room temperature and at frequencies below 200 MHz (highest frequency studied in this paper), in silicon resonators, Q_{p-p} is above 12 5000 [7]. Air damping could also be avoided through the operation of a resonator in partial vacuum. Ohmic loss could potentially be a major component of energy loss when the motional resistance of the resonator is comparable to the equivalent electrical resistance of the conductive signal path. However, this is not the case in this work as the resonators are not optimized for low motional resistance. On the other hand, anchor loss [8], [9] and interface loss [10], [11] are the main sources of loss in piezoelectric-on-silicon MEMS resonators. Specifically, anchor loss is believed to be a significant source of energy loss at the high end of very high-frequency (VHF) band. As the dimensions of the suspension tethers become comparable to the acoustic wavelength, a considerable amount of stress could be applied to tether resonator boundary in each cycle of vibration. This creates a stress wave which would propagate through the substrate transferring a portion of the acoustic energy from the resonating body to the substrate. Because the substrate is relatively large, the energy escaped through the tethers would be mostly scattered and damped in the substrate. Therefore, anchor loss is believed to be a significant source of loss in contour-mode resonators.

Manuscript received October 10, 2018; accepted January 9, 2019. Date of publication January 15, 2019; date of current version March 26, 2019. This work was supported by the National Science Foundation under Grant 1711632. *(Corresponding author: Sarah Shahraini.)*

S. Shahraini and R. Abdolvand are with the Department of Electrical Engineering and Computer Science, University of Central Florida, Orlando, FL 32816 USA (e-mail: sarah.shahraini@knights.ucf.edu).

M. Shahmohammadi is with Kionix Inc., Ithaca, NY 14850 USA.

H. Fatemi is with Qorvo, Apopka, FL 32703 USA.

Digital Object Identifier 10.1109/TUFFC.2019.2893121

A common approach to avoid excessive anchor loss is by placing the anchors at nodal points of the targeted resonance mode (i.e., regions with near-zero displacement on the acoustic cavity). Due to the near-zero displacement of these points, a minimal force would be exerted to the tether interface and anchor loss would be minimized [12]–[14]. The resonator/tether geometry and size could also be optimized to reduce the amount of acoustic energy lost through the tethers [8], [15]; however, such techniques are not effective when the tether is not located on the nodal points of the resonance mode shape. Alternatively, one could redesign the resonant cavity so that some of the acoustic energy escaping through the tethers is reflected back. This technique has been accomplished either by designing a phononic crystal structure close to (or on) the tethers [16], [17] or by utilizing structures which function as a classical acoustic reflector [9], [18], [19].

In this work, it is shown that silicon anisotropy could be exploited to minimize anchor loss for side-supported radial-mode thin-film piezoelectric-on-silicon (TPoS) disk resonators at VHF band. TPoS resonators have shown to offer some of the best $f.Q$ values among high-frequency MEMS resonators reported in the past [20] and contour-mode disk resonators are among the most attractive designs in [21] and [22]. One of the reasons for the popularity of this specific design is the symmetry of the resonant cavity which results in the center of the disk to be a node for all resonance modes; hence, high Q could be achieved by suspending the device from the center [21]. On the other hand, side-supported radial-mode disk resonators will have limited Q if not designed properly.

It is noteworthy that side-supported wine-glass-mode piezoelectric-based disk resonators has recently been studied in [23] and [24]. For these resonators, the resonator structure is supported from four minimum displacement points around the resonator and the anchor loss is managed by tether design optimization. However, with the exception of our recent publication [25], thin-film piezoelectric radial-mode disk resonators have not been studied as a center supported design was believed to be the only reasonable design for such modes, and the application of a center supported structure was deemed complicated. This work provides both theoretical and experimental evidence for viability of side-support radial-mode resonators on crystalline silicon and their performance superiority as the measured $f.Q$ figure of merit for the proposed side-supported radial-mode disk resonators is about four times higher than the side-supported wine-glass counterparts in [23] and about 40 times higher than those in [24], a testament to the effectiveness of our approach in minimizing anchor loss.

This paper aims to comprehensively explore the effect of anisotropy on the anchor loss in side-supported SCS disk resonators. It will be shown experimentally and through finite-element modeling that high-order harmonic radial-mode SCS disk resonators could be supported by tethers on the sides of the disk while maintaining a very high Q given the tethers are aligned to the [100] crystalline plane. The temperature dependence of frequency in the radial-mode SCS disk resonators fabricated on degenerately n-type doped substrates will also be studied and the temperature coefficient of frequency (TCF) curves are utilized to screen measured resonance peaks for identification of harmonic radial modes.

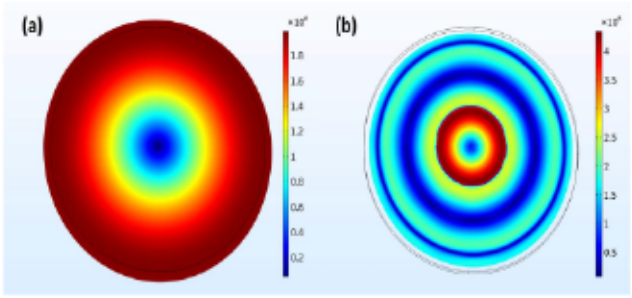

Fig. 1. Simulated total displacement for (a) first- and (b) fourth-harmonics radial resonance mode of a disk structure made from material with isotropic acoustic velocity. As seen, the only nodal point is in the center of the disk.

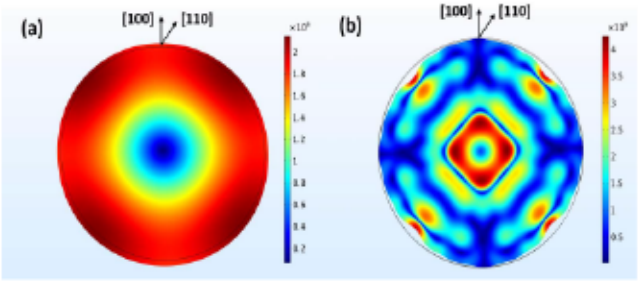

Fig. 2. Simulated total displacement for (a) first- and (b) fourth-harmonics radial resonance modes of a disk structure made on a [100] SCS substrate. Nodal points appear on the edges for higher harmonics (e.g., fourth-harmonic) along the [100] direction.

II. Analysis of the Radial Mode in SCS

The resonators studied in this work are designed to operate in the radial (a.k.a. breathing) resonance mode [22]. One of the most effective approaches to minimize anchor loss for this mode is to suspend the resonant body from the center of the disk where the displacement is virtually 0. However, from the fabrication point of view, center supported designs are hard to implement and specifically complicated to manufacture in TPoS structures as multiple isolated conductive paths have to be routed to the suspended structure through the central support stem. Thin-film piezoelectric resonators are commonly supported from the outer edges of the resonator body which is not typically considered an option with radial disk resonators.

For isotropic materials such as sputtered AlN, polycrystalline diamond, and polycrystalline silicon, the in-plane acoustic velocity is isotropic, and consequently, the displacement is uniform at the edge of the resonator body for a radial mode disk resonator, regardless of the harmonic number (as shown in Fig. 1). Therefore, there is no nodal point at the edge of the disk resonator and the only way to support the structure without substantially limiting the Q is to support it from the center.

A similar modal analysis reveals that contrary to the case for isotropic materials, for single-crystalline silicon (SCS), a nonuniform displacement field in the radial-mode disk resonators is established (Fig. 2). An SCS has a cubic symmetry and its effective Young's modulus is orientation dependent

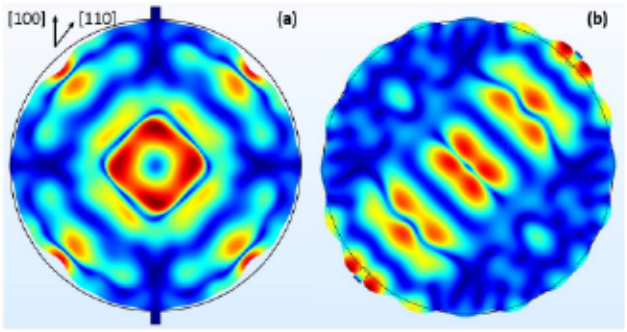

Fig. 3. Simulated total displacement for the fourth-order radial-mode SCS disk resonator with (a) tethers aligned to [100] plane and (b) tethers aligned to [110] plane with fixed boundary condition at the outer edges of the tethers. Radial mode shape is excessively distorted when the tethers are aligned to [110] crystalline plane.

and could vary up to 45% in different crystalline planes [26]. Main crystalline planes of SCS are [100], [110], and [111] and sound velocity in [110] direction is higher than sound velocity in [100] direction (7460 m/s in [100] and 8540 m/s in [110]).

As shown in Fig. 2, the total displacement of the disk edge is much larger in [110] direction compared to the [100] direction. This nonuniformity is more prominent for high-order harmonic resonance modes to the point that nodal points start to appear on the edges (e.g., fourth-harmonic in Fig. 2(b). We will exploit such nodal points to support the structure from the edges and, hence, preserving the Q. Results of modal analysis for fourth-harmonic radial mode disk resonators with suspension tethers aligned to [100] and [110] crystalline planes are shown in Fig. 3. As expected, tethers would excessively distort the mode shape for the radial-mode disk resonator on a [100] silicon wafer if the tethers are aligned to [110] crystalline plane. For the same resonator when tethers are aligned to [100] crystalline plane, the mode shape would be minimally affected and consequently the anchor loss is predicted to be minimized.

III. Finite-Element Modeling

A. Anchor Loss Modeling

MEMS resonators are often much smaller than the frame to which they are connected and as a result, the frame/substrate could be assumed a semi-infinite media. Although tethers are often at the nodal points, nevertheless, there is some periodic displacement at the resonator–tether boundary, which would transfer a portion of the acoustic energy to the substrate. The majority of this transferred acoustic wave would be scattered and dissipated rather than reflecting back to the resonant body.

There are few cases for which analytical studies exist on the energy loss of resonant systems through tethers. One such case is the bending mode clamped-free and clamped-clamped beam resonators [27]–[29]. These studies are mostly limited to anchor loss in beam resonators, and there are some simplifying assumptions made in all of them that further limits their application. Therefore, the usage of finite-element analysis in designing resonators with optimized anchor loss has become a necessity. The high-order absorption boundary condition and the perfectly matched layer (PML) are the most common approaches to model anchor loss [30]. PML modeling was first used for the electromagnetic wave propagation [31] and then generalized to all wave propagation with linear wave equations [30] and since has been used for modeling anchor loss for a variety of structures including disk resonators [32]. PML in the finite-element analysis is a layer of artificial material with a finite length that is placed on the boundaries of the substrate to which the resonant structure is connected. This layer is matched with the substrate so that there is no reflected acoustic wave from the interface boundary. There are two approaches for implementing PML; modifying material properties and coordinate stretching [33]. With complex coordinate change, the artificial layer is perfectly matched for all incident waves in all angles while for the material properties modification approach, the artificial layer is only matched for waves with 90° incident angle.

In this study, we used PML definition in COMSOL to simulate anchor loss for which the complex coordinate change is implemented internally. For the model to work properly, the PML region should be large enough to attenuate all the acoustic wave propagating through this medium [34]. It is also essential to choose proper PML parameters including PML scaling factor (α), substrate dimension, PML dimension, and mesh size to guarantee an accurate estimation for anchor quality factor [34]–[36]. PML scaling factor is used by COMSOL to produce an effective scaled width for PML for waves with incident angles other than 90° to compensate for longer wavelength seen by PML in the complex coordinate stretching method.

In 3-D modeling of a PML, for smooth dissipation of acoustic wave and to avoid reflection from PML, dissipation over a single mesh element should be limited [34]

$$\alpha k h < \frac{1}{5} \tag{2}$$

where α is the PML scaling factor, k is the wavenumber, and h is the element size. Choosing a large PML and small scaling factor or choosing a small PML and large scaling factor are two different ways to satisfy the requirement mentioned earlier. In [34], it was suggested to choose PML and substrate dimensions as a function of k

$$k W_s > \frac{1}{20} \sim \frac{1}{10} \tag{3}$$

$$k W_{\text{pml}} > \frac{1}{10} \sim \frac{1}{5} \tag{4}$$

where W_s is the substrate radius and W_{pml} is the PML radius. It is essential to model a big portion of the substrate in the low-frequency resonance modes to have an accurate model since the wavelength (λ) is large for low frequencies. On the other hand, for high-frequency resonances, modeling a small portion of the substrate would suffice.

In order to verify the validity of our PML model, anchor loss was first simulated for the in-plane bending mode of a clamped-free beam resonator and the results are compared with the analytical predictions. The quality factor for a bending mode cantilever beam could be estimated from (5) assuming that anchor loss is the dominant source of loss [28]

$$Q = A \frac{L}{T} \left(\frac{L}{V} \right)^4 \tag{5}$$

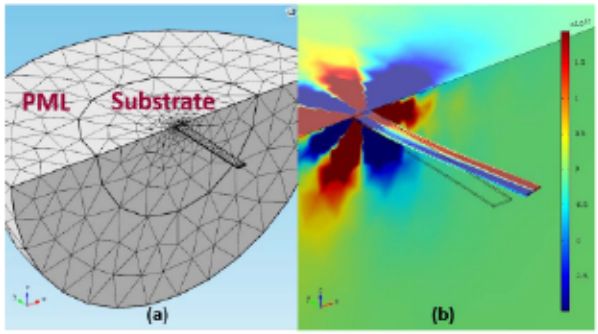

Fig. 4. (a) Meshed resonant structure and (b) stress field for the fundamental in-plane bending mode of a cantilever modeled in COMSOL for anchor loss analysis. The complex eigenfrequency is utilized to calculate the Q.

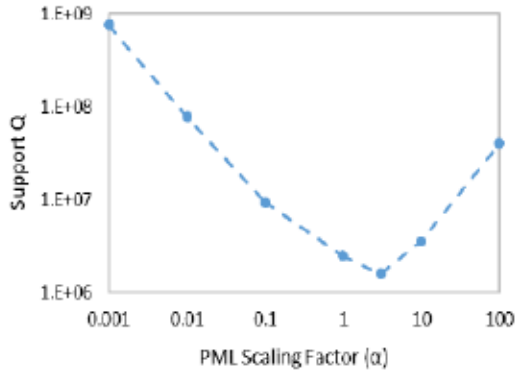

Fig. 5. Q_{anc} as a function of PML scaling factor for a cantilever beam resonator (similar to Fig. 4). The minimum Q is assumed to be the most accurate.

where L, V, and T are the beam length, width, and thickness, respectively, and A is a constant which changes with Poison ratio (e.g., $A = 3.175$ for $\upsilon = 0.33$, $A = 3.23$ for $\upsilon = 0.3$, and $A = 3.45$ for $\upsilon = 0.25$).

In COMSOL, the quality factor could be calculated from the complex eigenfrequencies resulted from a modal analysis that contains a source of loss [37], [38]

$$Q = \frac{\mathrm{Re}(f)}{2\mathrm{Im}(f)} \tag{6}$$

where $\mathrm{Re}(f)$ is the real part of the complex eigenfrequency and the $\mathrm{Im}(f)$ is its imaginary part.

The meshed structure and the stress filed for the fundamental in-plane bending mode of a cantilever beam resonator are shown in Fig. 4. The simulated quality factor is found to be dependent on the PML and substrate dimensions and PML scaling factor. From (3) and (4), we chose $W_s = (\lambda/10)$ and $W_{\mathrm{pml}} = (\lambda/5)$ and then tuned PML scaling factor to achieve the minimum Q. The dependence of Q on the PML scaling factor is presented in Fig. 5 and the lowest simulated value of Q is assumed to be the most accurate. The simulation and analytical results for several beam dimensions are compared in Table I and are in good agreement.

Next, the same PML model and procedure are used for the radial-mode TPoS disk resonator. The substrate and the PML radii are set to be equal to λ and 2λ, respectively. For each harmonic mode, the substrate and the PML radii are adjusted to the new wavelength and the PML scaling factor is tuned for minimum Q.

TABLE I
ANCHOR QUALITY FACTOR FOR BENDING MODE BEAM RESONATOR

Dimensions			Analytical anchor Q	Simulated anchor Q
L (μm)	V (μm)	T (μm)		
25	2.5	0.5	1.61×10^6	1.59×10^6
25	*1.25*	*0.5*	25.84×10^6	25.24×10^6
25	*2.5*	*0.25*	3.23×10^6	3.03×10^6
50	*2.5*	*0.5*	51.68×10^6	50.44×10^6

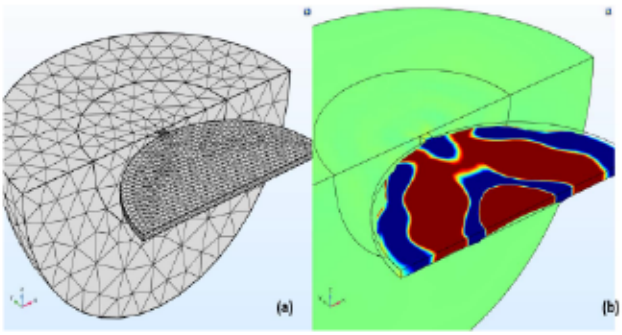

Fig. 6. (a) Meshed resonant structure and (b) stress field for a radial-mode TPoS disk resonator modeled in COMSOL for anchor loss analysis. The PML and the substrate radii are adjusted to λ and 2λ for each harmonic mode.

TABLE II
SIMULATED AND FABRICATED RESONATOR DIMENSIONS

	Radius (μm)	AlN thickness (μm)	Substrate thickness (μm)	Moly thickness (μm)
silicon resonator	160	0.5	8	0.2
UNCD resonator	160	0.5	3	0.2

In order to decrease computational load, a one-way symmetry is used for TPoS disk resonators and only half of the resonator is modeled. Meshing and stress field for radial mode disk resonators are shown in Fig. 6 and the simulated and fabricated TPOS disk resonator dimensions could be found in Table II.

The simulation is performed for resonators made of two different materials: ultrananocrystalline diamond (UNCD) (isotropic) and SCS (anisotropic) with suspension tethers aligned to [100] and [110] crystalline planes. Diamond resonators are studied to support the hypothesis that the sharp increase in the quality factor of the high-order mode silicon disk resonators when the tethers are rotated and aligned to [100] crystalline plane could be solely linked to the emergence of the peripheral nodal points. As shown by simulation, the same increase is not predicted in isotropic material (such as nanocrystalline diamond). The simulated quality factors (Q_{anc}) are presented in Table III.

The stress field for different harmonic orders of the radial-mode is plotted using a loss-less eigenfrequency

TABLE III
SIMULATED ANCHOR QUALITY FACTOR FOR RADIAL-MODE DISK RESONATORS

Harmonic #	Single Crystalline Silicon				UNC Diamond	
	Tethers aligned to [100]		Tethers aligned to [110]			
	f_0 (MHz)	Q (k)	f_0 (MHz)	Q (k)	f_0 (MHz)	Q (k)
Second	43.42	**0.46**	43.56	0.63	83.38	0.75
Third	68.93	**3.30**	69.44	0.88	133.08	0.86
Forth	94.77	**6.60**	95.35	0.62	-	-
Fifth	120.48	**33.26**	-	-	-	-
Eighth	196.33	**793.27**	-	-	-	-

**the mode shape was not found for the missing data points.*

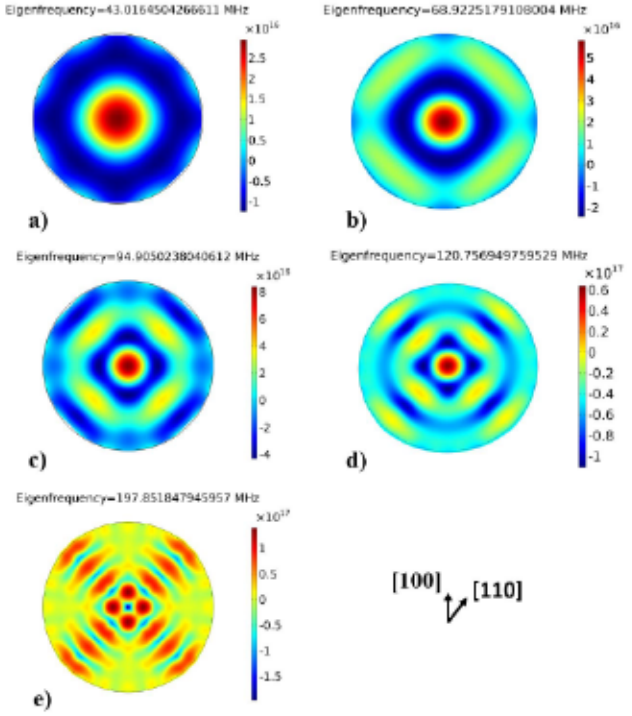

Fig. 7. Stress field for (a) second-, (b) third-, (c) fourth-, (d) fifth-, and (e) eighth-order radial mode disk resonator.

analysis in COMSOL (Fig. 7). The stress field in the x- and y-directions is added to plot the total stress field in the disk. The slight frequency difference between these simulated mode shapes and the values cited in Table III are due to the fact that for the simulated values in Table III, anchor loss is also considered (a substrate and a PML layer are added).

As expected, for TPoS resonators made of UNCD and also for resonators made of SCS with tethers aligned to the [110] plane, anchor loss is significant regardless of the harmonic number. On the other hand, for the silicon devices with tethers aligned to [100] plane, Q_{anc} is predicted to increase for higher order harmonic modes by orders of magnitude.

Finally, anchor loss is modeled for fourth-harmonic radial-mode TPoS resonators with different tether lengths and the simulated $Q's$ are compiled in Table IV. As seen, using the tether length as a parameter for optimizing anchor loss will not result in a significant improvement of Q if the tethers are aligned to [110] which further support the significance of the suggested approach in this work absent the efficiency of the alternative tether optimization methods.

TABLE IV
SIMULATED SUPPORT Q FOR TETHER WITH VARIABLE LENGTH

	Tether aligned to [100]				Tether aligned to [110]			
Tether length	11μm	2λ/8	3λ/8	4λ/8	11μm	2λ/8	3λ/8	4λ/8
4th Harmonic Q (k)	6.6	1.9	5.9	3.2	0.6	0.8	1.6	0.7

B. TCF Modeling

To predict the frequency drift versus temperature for radial mode SCS disk resonators, eigenfrequency analysis is utilized in COMSOL. Frequency drift versus temperature curves are generated for radial-mode disk resonators and also for bulk extensional modes in [100] and [110] aligned block resonators, fabricated on the same substrate.

The stiffness coefficients and their corresponding temperature coefficients for Phosphorous-doped SCS ($n = 6 \times 10^{19}$ cm^{-3}) are borrowed from [39] (Table V) [$T_C^{(1)}$ is the first-order temperature coefficient of elastic constant and $T_C^{(2)}$ is the second-order temperature coefficient of elastic constant]. The stiffness matrix is then calculated for each temperature and is used to repeat the modal analysis and calculate the shifted resonance frequency.

As shown in Fig. 8, the turn-over temperature for the radial-mode disk resonator is predicted to be between the turn-over temperatures of block resonators aligned to [100] and [110] crystalline planes [40]. In radial-mode disk resonators, there are significant stress field components in both [100] and [110] crystalline planes and, therefore, the predicted temperature-frequency dependence is reasonable.

TABLE V

ELASTIC CONSTANTS OF PHOSPHORUS-DOPED ($n = 6 \times 10^{19}$ cm^{-3}) SILICON AND THEIR CORRESPONDING FIRST- AND SECOND-ORDER TEMPERATURE COEFFICIENTS [39]

Dopant	C_{11} (GPa)	C_{12} (GPa)	C_{44} (GPa)	$T_{C_{11}}^{(1)}$ (ppm/°C)	$T_{C_{12}}^{(1)}$ (ppm/°C)	$T_{C_{44}}^{(1)}$ (ppm/°C)	$T_{C_{11}}^{(2)}$ (ppb/°C^2)	$T_{C_{12}}^{(2)}$ (ppb/°C^2)	$T_{C_{44}}^{(2)}$ (ppb/°C^2)
Phosphorus $6.6 \times 10^{19} cm^{-3}$	164.0	66.7	78.2	-34.2	-135.2	-67.8	-103	-1	-40

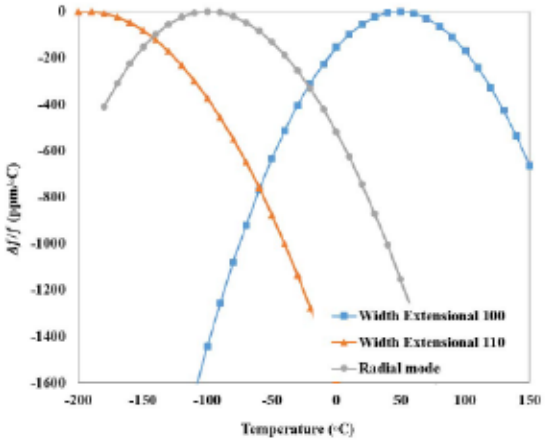

Fig. 8. Simulated temperature–frequency dependence for radial mode disk resonator fabricated on n-type doped silicon ($n = 6 \times 10^{19}$ cm^{-3}) compared with width-extensional resonators oriented in two different directions.

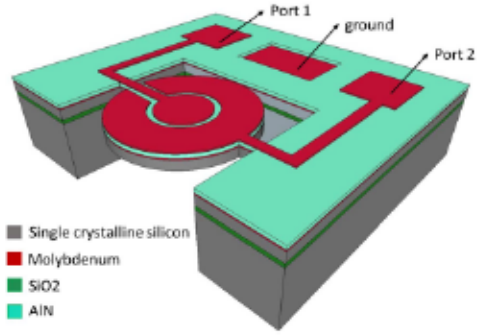

Fig. 9. Schematic of a TPoS disk resonator fabricated in this study.

IV. FABRICATION PROCESS

TPoS resonators are constituted of a piezoelectric layer sandwiched between two metal layers and deposited on a layer of low acoustic loss material. The piezoelectric layer is actuated by an applied electric field across the metal electrodes. A schematic of the TPoS disk resonator of this work is shown in Fig. 9. The radial-mode disk resonators of this work are fabricated both on SCS and UNCD device layers.

Resonators with the silicon device layers are fabricated on an 8-μm silicon-on-insulator (SOI) wafer using a five-mask fabrication process. The fabrication process flow is shown in Fig. 10. First, the stack of Molybdenum-AlN-Molybdenum is sputtered on an SOI wafer. Then, the top Molybdenum layer is dry etched to shape the top electrodes [Fig. 10(a)]. Next, the AlN film is wet-etched to create access to the bottom

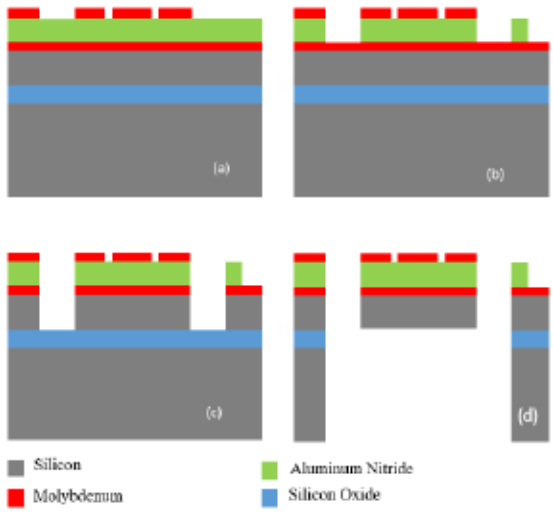

Fig. 10. Schematic process flow for fabrication of the disk resonators on an SOI wafer.

metal layer [Fig. 10(b)]. The resonator body is then defined by successive plasma etching of the full stack of material down to the SOI buried oxide (BOX) layer [Fig. 10(c)]. Handle layer silicon is then etched from the backside in a deep-reactive-ion-etching chamber and the resonator is finally released by wet etching the BOX layer in buffered oxide etchant [Fig. 10(d)]. The detailed process flow for devices made on the SCS device layer could be found in [41].

Disk resonators are also fabricated on UNCD. A UNCD film with an average grain size of less than 10 nm was deposited by hot filament chemical vapor deposition. To promote C-plane grain growth in the following sputtered AlN layer, UNCD deposition is followed by two polishing steps. The rest of the process is very similar to the fabrication steps on an SOI wafer explained earlier. The diamond layer is etched in an inductively coupled plasma etching chamber with O_2/CF_4 plasma. The detailed process flow for devices made on UNCD device layer could be found in [42].

V. EXPERIMENTAL RESULTS

A. Quality Factor Measurements

The frequency response of the TPoS disk resonators is measured both in atmospheric pressure and partial vacuum (1 torr) using a Rohde & Schwarz ZNB 8 network analyzer and a pair of ground signal ground (GSG) probes (Cascade Microtech Inc., a subsidiary of FormFactor, Livermore, CA, USA) at

TABLE VI
MEASURED QUALITY FACTOR DATA FOR RADIAL MODE DISK RESONATORS

Harmonic #	single crystalline silicon								UNC Diamond			
	Tethers aligned to [100]				Tethers aligned to [110]							
	f_0 (MHz)	Q_{max} (k)	R_m (kΩ)	Q_{avg} (k)	f_0 (MHz)	Q_{max} (k)	R_m (kΩ)	Q_{avg} (k)	f_0 (MHz)	Q_{max} (k)	R_m (kΩ)	Q_{avg} (k)
Second	42.8	**0.4**	6.0	**0.3**	43.3	0.5	20.3	0.5	80.0	0.9	6.1	0.7
Third	69.0	**2.8**	0.3	**1.8**	70.2	0.65	7.7	0.47	128.1	0.2	9.4	0.17
Forth	94.7	**5.6**	1.0	**3.8**	95.9	0.8	33.1	0.65	-	-	-	-
Fifth	120.3	**7.4**	1.0	**4.3**	-	-	-	-	-	-	-	-
Eighth	195.8	**9.7**	1.2	**6.3**	-	-	-	-	-	-	-	-

ambient temperature while terminated with the internal 50-Ω impedance of the network analyzer. The loaded quality factors (Q_{loaded}) are measured and the unloaded quality factors are extracted by deembedding the loading effect of the termination resistances.

Frequency responses are measured for disk resonators on anisotropic (SCS) device layer with tethers aligned to [100] and [110] crystalline planes and also for the disk resonators fabricated on isotropic UNCD device layer.

As expected, resonance frequencies for the UNCD disk resonators are higher compared to the higher Young's modulus of the UNCD [42].

As shown in Table VI, for the UNCD disk resonators and also the SCS disk resonator with tethers aligned to [110] direction, Q values are relatively low. This is believed to support our hypothesis indicating that a large portion of acoustic energy would be lost through tethers considering that the structure was not supported from its nodal points in these resonators. On the other hand, for higher harmonic radial-mode disk resonators with tethers aligned to [100] plane, unloaded quality factor improves from an average of 290 at 43 MHz to 6300 at 196 MHz for the eighth-harmonic mode. Frequency responses are measured in atmospheric pressure for five SCS disk resonators with [100]-aligned tethers and five UNCD disk resonators. The maximum quality factor (Q_{max}) and the average quality factor (Q_{avg}) are reported in Table VI. For the SCS resonators with [110]-aligned tethers, only two resonators exhibited peaks around the expected resonance frequencies and the average data were reported for those two resonators.

The typical frequency response for a UNCD and an SCS radial-mode TPoS disk resonator with tethers aligned to [100] crystalline plane are shown in Figs. 11 and 12, respectively. The frequency span for these measurements is 40–200 MHz and several harmonics of radial mode are identified for these devices (inset figures on the frequency Figs. 11 and 12). The anchor quality factor is modeled for all the resonance modes within a region around the measured resonance frequencies for each harmonic mode. For the mode shapes with a reasonable quality factor, the TCF curves are modeled and compared

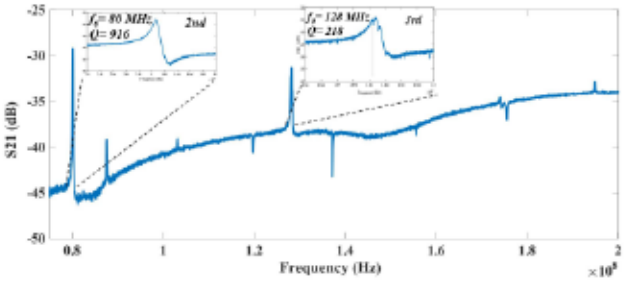

Fig. 11. Recorded $S21$ for a UNCD radial-mode TPoS disk resonator simultaneously presenting the resonance peaks of second, third harmonics with their corresponding Q.

to the measured TCF curve to confirm that the measured resonance peaks are assuredly higher order harmonic radial modes.

For the SCS resonators with [110]-aligned tethers, the simulated and measured quality factors are matched fairly well. This confirms our hypothesis that the anchor loss is the dominant source of loss for the side-supported radial mode TPoS resonators when the structure is not supported from its nodal points. However, considering the simulated quality factor for the higher order harmonic radial mode TPoS resonators with [100]-aligned tethers, the anchor loss is almost eliminated. For these resonators, we believe other sources of loss such as interface loss and surface loss are playing a more important role.

It is necessary to mention that the top electrode pattern in these resonators is not designed for the optimum coupling factor. For high harmonic modes, a portion of electrical charge accumulated under the electrodes will be canceled out since areas with opposing stress polarity are covered with the same electrode. On the other hand, with such electrode design, several harmonic numbers of the radial modes could be excited on the same resonator and the quality factor could be fairly compared for all such harmonic radial mode TPoS resonators.

The unloaded quality factors measured both at atmospheric pressure and partial vacuum for different harmonics of the radial-mode TPoS disk resonator exhibiting the highest Q are

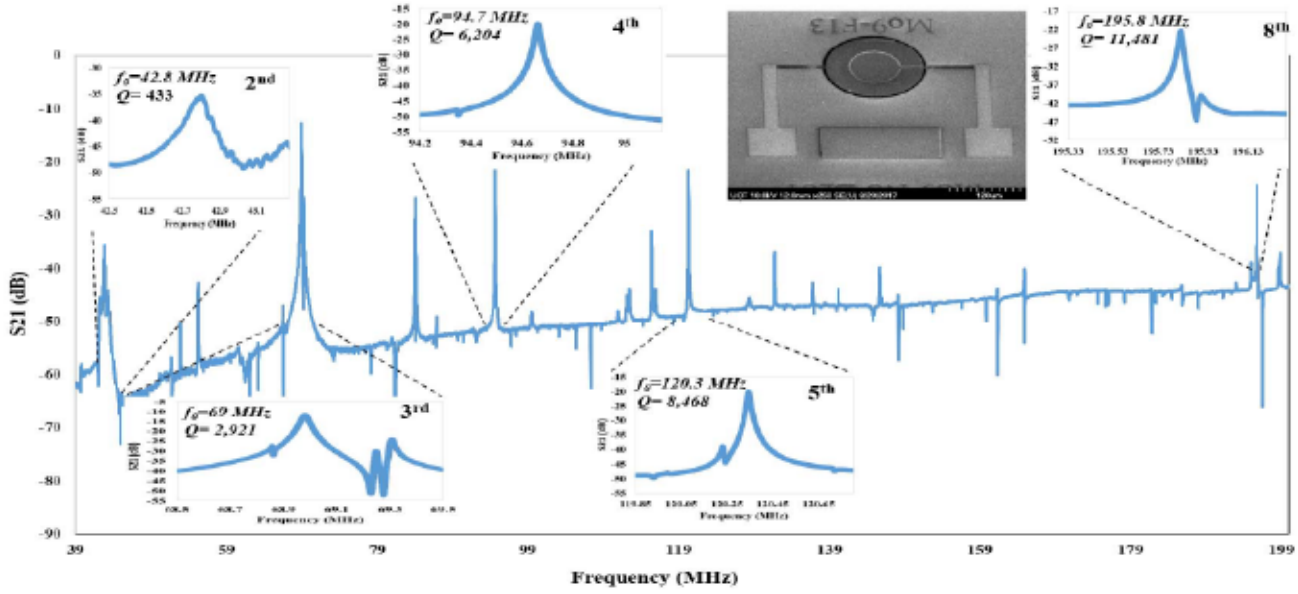

Fig. 12. Recorded $S21$ for an SCS radial-mode TPoS disk resonator with tethers aligned to [100] plane measured in partial vacuum simultaneously presenting the resonance peaks of second, third, fourth, fifth, and eighth harmonics with their corresponding Q.

TABLE VII

MEASURED DATA FOR SINGLE CRYSTALLINE SILICON DISK RESONATOR WITH TETHERS ALIGNED TO [100] DIRECTION

Harmonic #	In Atmospheric pressure			In partial Vacuum (1 Torr)		
	f_0 (MHz)	Q (k)	R_m (kΩ)	f_0 (MHz)	Q (k)	R_m (kΩ)
Second	42.78	0.43	6.04	42.78	0.45	5.79
Third	68.98	2.80	0.31	68.98	2.92	0.29
Forth	94.66	5.60	1.01	94.66	6.20	0.90
Fifth	120.34	7.44	0.98	120.34	8.47	0.91
Eighth	**195.82**	**9.66**	**1.22**	**195.82**	**11.48**	**1.20**

TABLE VIII

COMPARISON OF THE BEST RESULT REPORTED IN THIS WORK WITH SELECT PUBLISHED DATA IN THE SAME FREQUENCY RANGE

Resonator Type	f_0 (MHz)	Q_{air} (K)	Q_{vac} (K)	Resonance mode	Reference
TPOS	195.82	9.66	11.48	Radial	This work
TPOS	142	6.8	-	Lateral extensional	[44]
Capacitive	193	8.8	23	Radial	[22]
Piezoelectric	229.9	-	4.3	Lateral extensional	[45]

compared in Table VII. For lower harmonic modes, it appears that the quality factors do not change significantly under vacuum which further confirms that the anchor loss is the dominant source of loss for the second and third harmonics. For the high-order modes, on the other hand, the anchor loss is no longer the main source of loss and the quality factor improves about 19% in vacuum in the absence of air damping loss for eighth-harmonic mode (increased from 9660 to 11 480).

The quality factor of the eighth-harmonic radial-mode TPoS resonator is compared to several other published results from resonators in the same range of frequencies (Table VIII). As seen here, the quality factor of the TPoS disk resonator (this work) is the second best only after the capacitive resonators while the $kt^2.Q$ in this device surpasses that of the capacitive resonator by a large margin. Also, it is notable that for a capacitive resonator, the quality factor improves significantly when measured in the vacuum. This is because squeezed-film air damping is one of the main sources of loss in the capacitive resonators due to the extremely small size of the capacitive gaps that are necessary for improving the coupling factor [43]. This sensitivity to air damping will put stringent requirement on the packaging of such resonators that could be relaxed for TPoS resonators.

B. TCF Measurements

The TCF is measured for a radial-mode TPoS resonator and lateral-extensional mode TPoS resonators aligned to [100] and [110] planes. The center frequency drift is measured in the range of −60 °C–80 °C in a Janis cryogenic vacuum probe station in which liquid nitrogen is used to cool down the chuck below ambient temperatures. The results are plotted in Fig. 13. All three devices used for this measurement are made on the same substrate with a doping concentration of $n \sim 4 \times 10^{19}$ cm^{-3}. As predicted by the simulation results of Section III-B, the turn-over temperature for the radial-mode disk is between the two turn-over temperatures for the extensional mode resonators aligned to [100] and [110]. However, the turn-over temperature for all three resonator types is at lower temperatures than predicted in Fig. 8. This is mainly because the available stiffness coefficients used for

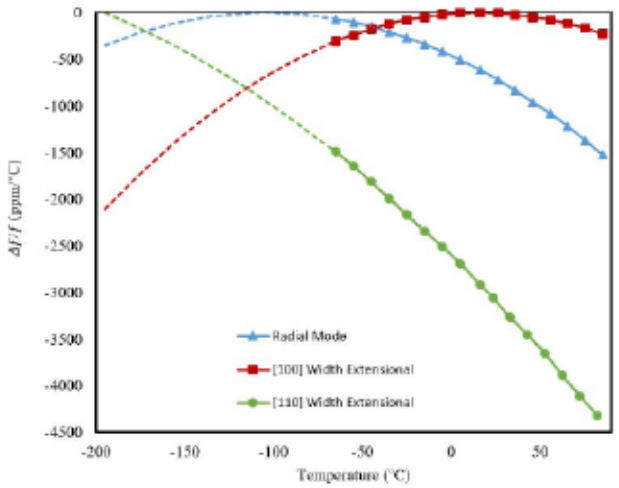

Fig. 13. Frequency–temperature plot measured for a radial-mode TPoS disk resonator and extensional mode TPoS resonators aligned to [100] and [110] silicon planes.

the simulation section are reported for a doping concentration higher than what was used for fabrication in this work and also only the silicon layer was considered in the simulation and the contribution of AlN and Molybdenum layers were neglected in the simulation. For the radial-mode disk resonator, the extrapolated turn-over temperature is at ~ -105 °C, when it is at ~16 °C for the [100] extensional mode resonator and below −200 °C for the [110] extensional mode resonator.

VI. Conclusion

Radial-mode disk resonators are commonly supported from the center of the disk due to the expected excessive anchor loss for side-supported radial modes. Therefore, piezoelectric radial-mode disk resonators are seldom developed. In this work, it was demonstrated that in a TPoS radial-mode disk resonator by rotating the anchors to align with [100] plane, anchor loss would be reduced significantly. Specifically, anchor loss would no longer be the dominant source of loss for high-order harmonic modes. Devices are fabricated on SCS and UNCD and the validity of this claim is confirmed both with experimental measurements and finite-element simulations. Due to their reported high-quality factor, high-order radial-mode TPoS disk resonators are excellent candidates for stable oscillator designs in VHF band.

References

[1] R. Abdolvand, B. Bahreyni, J. E.-Y. Lee, and F. Nabki, "Micromachined resonators: A review," *Micromachines*, vol. 7, no. 9, p. 160, Sep. 2016.

[2] J. T. M. van Beek and R. Puers, "A review of MEMS oscillators for frequency reference and timing applications," *J. Micromech. Microeng.*, vol. 22, no. 1, p. 13001, 2012.

[3] H. Lee, A. Partridge, and F. Assaderaghi, "Low jitter and temperature stable MEMS oscillators," in *Proc. IEEE Int. Freq. Control Symp.*, Baltimore, MD, USA, May 2012, pp. 1–5.

[4] R. Abdolvand, H. Fatemi, and S. Moradian, "Quality factor and coupling in piezoelectric MEMS resonators," in *Piezoelectric MEMS Resonators*, 1st ed. Cham, Switzerland: Springer, 2017, pp. 133–152.

[5] T. O. Woodruff and H. Ehrenreich, "Absorption of sound in insulators," *Phys. Rev.*, vol. 123, no. 5, p. 1553, 1961.

[6] A. S. Nowick, *Anelastic Relaxation in Crystalline Solids*, vol. 1. Amsterdam, The Netherlands: Elsevier, 2012.

[7] R. Tabrizian, M. Rais-Zadeh, and F. Ayazi, "Effect of phonon interactions on limiting the $f.Q$ product of micromechanical resonators," in *Proc. Int. Solid-State Sens., Actuators Microsyst. Conf. (TRANSDUCERS)*, Denver, CO, USA, 2009, pp. 2131–2134.

[8] J. Segovia-Fernandez, M. Cremonesi, C. Cassella, A. Frangi, and G. Piazza, "Anchor losses in AlN contour mode resonators," *J. Microelectromech. Syst.*, vol. 24, no. 2, pp. 265–275, 2015.

[9] B. P. Harrington and R. Abdolvand, "In-plane acoustic reflectors for reducing effective anchor loss in lateral–extensional MEMS resonators," *J. Micromech. Microeng.*, vol. 21, no. 8, p. 085021, 2011.

[10] S. Gong, N.-K. Kuo, and G. Piazza, "GHz AlN lateral overmoded bulk acoustic wave resonators with a $f \cdot Q$ of 1.17×10^{13}," in *Proc. Joint Conf. IEEE Int. Freq. Control Eur. Freq. Time Forum (FCS)*, San Francisco, CA, USA, May 2011, pp. 1–5.

[11] Z. Hao and B. Liao, "An analytical study on interfacial dissipation in piezoelectric rectangular block resonators with in-plane longitudinal-mode vibrations," *Sens. Actuators A, Phys.*, vol. 163, no. 1, pp. 401–409, 2010.

[12] K. Wang, A.-C. Wong, and C. T.-C. Nguyen, "VHF free-free beam high-Q micromechanical resonators," *J. Microelectromech. Syst.*, vol. 9, no. 3, pp. 347–360, 2000.

[13] J. Wang, Z. Ren, and C. T.-C. Nguyen, "1.156-GHz self-aligned vibrating micromechanical disk resonator," *IEEE Trans. Ultrason., Ferroelectr., Freq. Control*, vol. 51, no. 12, pp. 1607–1628, Dec. 2004.

[14] S.-S. Li, Y.-W. Lin, Y. Xie, Z. Ren, C. T.-C. Nguyen, "Micromechanical 'hollow-disk' ring resonators," in *Proc. 17th IEEE Int. Conf. Micro Electro Mech. Syst.*, Jan. 2004, pp. 821–824.

[15] J. E.-Y. Lee, J. Yan, and A. A. Seshia., "Study of lateral mode SOI-MEMS resonators for reduced anchor loss," *J. Micromech. Microeng.*, vol. 21, no. 4, p. 045010, 2011.

[16] F.-C. Hsu, J.-C. Hsu, T.-C. Huang, C.-H. Wang, and P. Chang, "Design of lossless anchors for microacoustic-wave resonators utilizing phononic crystal strips," *Appl. Phys. Lett.*, vol. 98, no. 14, p. 143505, 2011.

[17] L. Sorenson, J. L. Fu, and F. Ayazi, "One-dimensional linear acoustic bandgap structures for performance enhancement of AlN-on-Silicon micromechanical resonators," in *Proc. 16th Int. Solid-State Sens., Actuators Microsyst. Conf. (TRANSDUCERS)*, 2011, pp. 918–921.

[18] V. Tas, S. Olcum, M. D. Aksoy, and A. Atalar, "Reducing anchor loss in micromechanical extensional mode resonators," *IEEE Trans. Ultrason., Ferroelectr., Freq. Control*, vol. 57, no. 2, pp. 448–454, Feb. 2010.

[19] M. Pandey, R. B. Reichenbach, A. T. Zehnder, A. Lal, and H. G. Craighead, "Reducing anchor loss in MEMS resonators using mesa isolation," *J. Microelectromech. Syst.*, vol. 18, no. 4, pp. 836–844, Aug. 2009.

[20] B. P. Harrington, M. Shahmohammadi, and R. Abdolvand, "Toward ultimate performance in GHZ MEMS resonators: Low impedance and high Q," in *Proc. IEEE 23rd Int. Conf. Micro Electro Mech. Syst. (MEMS*, Wanchai, Hong Kong, Jan. 2010, pp. 707–710.

[21] R. A. Schneider and C. T.-C. Nguyen, "On/off switchable high-Q capacitive-piezoelectric AlN resonators," in *Proc. IEEE 27th Int. Conf. Micro Electro Mech. Syst. (MEMS)*, Jan. 2014, pp. 1265–1268

[22] J. R. Clark, W.-T. Hsu, M. A. Abdelmoneum, and C. T.-C. Nguyen, "High-Q UHF micromechanical radial-contour mode disk resonators," *J. Microelectromech. Syst.*, vol. 14, no. 6, pp. 1298–1310, Dec. 2005.

[23] M. Y. Elsayed, P. V. Cicek, F. Nabki, and M. N. El-Gamal, "Bulk mode disk resonator with transverse piezoelectric actuation and electrostatic tuning," *J. Microelectromech. Syst.*, vol. 25, no. 2, pp. 252–261, Apr. 2016.

[24] M. Y. Elsayed and F. Nabki, "Piezoelectric bulk mode disk resonator post-processed for enhanced quality factor performance," *J. Microelectromech. Syst.*, vol. 26, no. 1, pp. 75–83, Feb. 2017.

[25] S. Shahraini, M. Shahmohammadi, and R. Abdolvand, "Support loss evasion in breathing-mode high-order silicon disc resonators," in *Proc. IEEE Int. Ultrason. Symp. (IUS)*, Washington, DC, USA, Sep. 2017, pp. 1–4.

[26] M. A. Hopcroft, W. D. Nix, and T. W. Kenny, "What is the Young's Modulus of Silicon?" *J. Microelectromech. Syst.*, vol. 19, no. 2, pp. 229–238, 2010.

[27] Y. Jimbo and K. Itao, "Energy loss of a cantilever vibrator," (in Japanese), *J. Horological Inst. Jpn.*, vol. 47, pp. 1–15, Jan. 1968.

[28] J. A. Judge, D. M. Photiadis, J. F. Vignola, B. H. Houston, and J. Jarzynski, "Attachment loss of micromechanical and nanomechanical resonators in the limits of thick and thin support structures," *J. Appl. Phys.*, vol. 101, no. 1, p. 013521, 2007.

[29] Z. Hao, A. Erbil, and F. Ayazi, "An analytical model for support loss in micromachined beam resonators with in-plane flexural vibrations," *Sens. Actuators A, Phys.*, vol. 109, no. 1, pp. 156–164, 2003.
[30] D. Rabinovich, D. Givoli, and E. Bécache, "Comparison of high-order absorbing boundary conditions and perfectly matched layers in the frequency domain," *Int. J. Numer. Methods Biomed. Eng.*, vol. 26, no. 10, pp. 1351–1369, 2010.
[31] J.-P. Berenger, "A perfectly matched layer for the absorption of electromagnetic waves," *J. Comput. Phys.*, vol. 114, no. 2, pp. 185–200, 1994.
[32] U. Basu and A. K. Chopra, "Perfectly matched layers for time-harmonic elastodynamics of unbounded domains: Theory and finite-element implementatio," *Comput. Methods Appl. Mech. Eng.*, vol. 192, no. 11, pp. 1337–1375, 2003
[33] W. C. Chew, J. M. Jin, and E. Michielssen, "Complex coordinate system as a generalized absorbing boundary condition," *IEEE Antennas Propag. Soc. Int. Symp. Dig.*, Montreal, QC, Canada, vol. 3, Jul. 1997, pp. 2060–2063.
[34] A. Frangi, A. Bugada, M. Martello, and P. T. Savadkoohi, "Validation of PML-based models for the evaluation of anchor dissipation in MEMS resonators," *Eur. J. Mech.-A/Solids*, vol. 37, pp. 256–265, Jan./Feb. 2013.
[35] D. D. Gerrard, E. J. Ng, C. H. Ahn, V. A. Hong, Y. Yang, and T. W. Kenny, "Modeling the effect of anchor geometry on the quality factor of bulk mode resonators," in *Proc. 18th Int. Conf. Solid-State Sens., Actuators Microsyst. (TRANSDUCERS)*, 2015, pp. 1997–2000.
[36] V. Thakar and M. Rais-Zadeh, "Optimization of tether geometry to achieve low anchor loss in Lamé-mode resonatorss," in *Proc. Joint Eur. Freq. Time Forum Int. Freq. Control Symp. (EFTF/IFC)*, 2013, pp. 129–132.
[37] P. G. Steeneken, J. J. M. Ruigrok, S. Kang, J. T. M. van Beek, J. Bontemps, and J. J. Koning. (2013). "Parameter extraction and support-loss in MEMS resonators." [Online]. Available: https://arxiv.org/abs/1304.7953
[38] R. Abdolvand, J. Gonzales, and G. Ho, "Finite element modeling of resonators," in *Resonant MEMS: Fundamentals, Implementation and Application*, 1st ed. Hoboken, NJ, USA: Wiley, 2015.
[39] E. J. Ng, V. A. Hong, Y. Yang, C. H. Ahn, C. L. M. Everhart, and T. W. Kenny, "Temperature dependence of the elastic constants of doped silicon," *J. Microelectromech. Syst.*, vol. 24, no. 3, pp. 730–741, 2015.
[40] M. Shahmohammadi, B. P. Harrington, and R. Abdolvand, "Turnover temperature point in extensional-mode highly doped silicon microresonators," *IEEE Trans. Electron Devices*, vol. 60, no. 3, pp. 1213–1220, Mar. 2013.
[41] R. Abdolvand, H. M. Lavasani, G. K. Ho, and F. Ayazi, "Thin-film piezoelectric-on-silicon resonators for high-frequency reference oscillator applications," *IEEE Trans. Ultrason., Ferroelectr., Freq. Control*, vol. 55, no. 12, pp. 2596–2606, Dec. 2008.
[42] H. Fatemi and R. Abdolvand, "Low-loss lateral-extensional piezoelectric filters on ultrananocrystalline diamond," *IEEE Trans. Ultrason., Ferroelectr., Freq. Control*, vol. 60, no. 9, pp. 1978–1988, Sep. 2013.
[43] M. Bao and H. Yang, "Squeeze film air damping in MEMS," *Sens. Actuators A, Phys.*, vol. 136, no. 1, pp. 3–27, 2007.
[44] H. Zhu and J. E.-Y. Lee, "Design of phononic crystal tethers for frequency-selective quality factor enhancement in AlN piezoelectricon-silicon resonators," in *Proc. Eurosens. Conf.*, Freiburg, Germany, Sep. 2015, pp. 516–519.
[45] G. Piazza, P. J. Stephanou, and A. P. Pisano, "Piezoelectric aluminum nitride vibrating contour-mode MEMS resonators," *J. Microelectromech. Syst.*, vol. 15, no. 6, pp. 1406–1418, Dec. 2006.

Sarah Shahraini (GS'17) received the B.Sc. and M.Sc. degrees in electrical engineering from the K. N. Toosi University of Technology, Tehran, Iran, in 2010 and 2012, respectively. She is currently pursuing the Ph.D. degree with the University of Central Florida, Orlando, FL, USA.

Her research interests lie in the area of microelectro-mechanical systems with a special focus on design, fabrication, and characterization of microresonators for stable oscillator, filter, and sensor applications.

Mohsen Shahmohammadi received the B.Sc. degree in electrical engineering from the Isfahan University of Technology, Isfahan, Iran, in 1995, the M.Sc. degree in electrical engineering from the K. N. Toosi University of Technology, Tehran, Iran, in 1999, and the Ph.D. degree from the School of Electrical and Computer Engineering, Oklahoma State University, Tulsa, OK, USA, in 2013.

In 2009, he joined Oklahoma State University. He is currently a Senior MEMS Design Engineer with Kionix Inc., Ithaca, NY, USA.

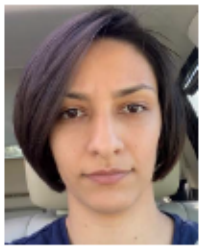

Hedy Fatemi received the B.S. degree in electrical engineering from the University of Tehran, Tehran, Iran, in 2009, the M.S. degree in electrical engineering from Oklahoma State University, Stillwater, OK, USA, in 2011, and the Ph.D. degree, with a focus on piezoelectric resonant devices, from the University of Central Florida, Orlando, FL, USA, in 2015.

She is currently a Filter Design and Development Engineer with Qorvo, Apopka, FL, USA.

Reza Abdolvand (A'08–M'09–SM'18) received the Ph.D. degree from the School of Electrical and Computer Engineering, Georgia Institute of Technology, Atlanta, GA, USA, in 2008.

He was an Assistant Professor with the School of Electrical and Computer Engineering, Oklahoma State University, Stillwater, OK, USA. In 2014, he joined the University of Central Florida, Orlando, FL, USA, where he is currently an Associate Professor and the Director of the Dynamic Microsystems Laboratory, Department of Electrical Engineering and Computer Science. He has authored or coauthored two book chapters and more than 70 peer-reviewed journal and conference articles in his field of expertise. He holds 12 U.S. patents. His research interests are in the general area of micro/nanoelectromechanical systems with over 15 years of experience in design, fabrication, and characterization of microresonators with applications in radio frequency circuits and resonant sensors including biosensors.

Dr. Abdolvand was a recipient of the National Aeronautics and Space Administration Patent Application Award in 2009.